

Imaging corneal pathology in a transgenic mouse model using nonlinear microscopy

Julia G. Lyubovitsky

University of California
Beckman Laser Institute
Laser Microbeam and Medical Program
Irvine, California 92612

Joel A. Spencer

University of California
Departments of Medicine and Biological Chemistry
Irvine, California 92697

Tatiana B. Krasieva

University of California
Beckman Laser Institute
Laser Microbeam and Medical Program
Irvine, California 92612

Bogi Andersen

University of California
Departments of Medicine and Biological Chemistry
Irvine, California 92697

Bruce J. Tromberg

University of California
Beckman Laser Institute
Laser Microbeam and Medical Program
Irvine, California 92612
E-mail: bjtrombe@uci.edu

Abstract. A transgenic mouse model with a Clim [co-factor of LIM (a combination of first letters of Lin-11 (*C. elegans*), ISL1 (rat), and Mec-3 (*C. elegans*) gene names) domain proteins] gene partially blocked in the epithelial compartment of its tissues is used to establish the sensitivity of intrinsic reflectance nonlinear optical microscopy (NLOM) to stromal and cellular perturbations in the cornea. Our results indicate dysplasia in the squamous epithelium, irregular collagen arrays in the stroma, and a compromised posterior endothelium in the corneas of these mice. As suggested by biochemical data, the collagen alterations are likely due to collagen III synthesis and deposition during healing and remodeling of transgenic mice corneal stromas. All of the topographic features seen in NLOM images of normal and aberrant corneas are confirmed by coregistration with histological sections. In this work, we also use ratiometric redox fluorometry based on two-photon excited cellular fluorescence from reduced nicotinamide adenine dinucleotide (NAD)(P)H and oxidized flavin adenine dinucleotide (FAD) to study mitochondrial energy metabolism. Employing this method, we detect higher metabolic activity in the endothelial layer of cornea compared to an epithelial layer located further away from the metabolites. The combination of two-photon excited fluorescence (TPF) with second harmonic generation (SHG) signals allows imaging to aid in understanding the relationship between alternation of specific genes and structural changes in cells and extracellular matrix. © 2006 Society of Photo-Optical Instrumentation Engineers. [DOI: 10.1117/1.2163254]

Keywords: cornea; microscopy; two photon; collagen; mitochondria; metabolism.

Paper 05127 received May 25, 2005; accepted for publication Sep. 1, 2005; published online Jan. 31, 2006.

1 Introduction

Cornea is a transparent tissue covering the front surface of the eye. It protects the eye from foreign matter and delivers two thirds of the eye's refractive power. To remain clear, cornea is devoid of any blood vessels, and is nourished by a tear film and an aqueous humor filling the chamber behind it. The arrangement, spacing, and size of collagen fibers in corneal stroma are critical in maintaining corneal transparency.¹ Microbial keratitis, ocular herpes, a range of corneal dystrophies, and complications due to refractive surgeries are among many causes of corneal scars leading to permanent vision loss. Therefore, being able to visualize individual cells and collagen matrix at submicron resolution noninvasively *in vivo* is important in understanding the biology of normal corneas and evaluating their transformation during disease and wound healing.

In the last few years, a combination of nonlinear signals such as intrinsic two-photon fluorescence (TPF) and second harmonic generation (SHG) has been employed to form high

contrast images of cells and extracellular matrix.^{2–10} Previous nonlinear optical microscopy (NLOM) studies hinted at the possibility of employing endogenous fluorescence¹¹ and second harmonic generation (SHG) signals to analyze corneal health,¹² particularly during/after intrastromal corneal surgery.^{13,14} Yet currently, no clear relationship between the observed intrinsic NLOM signals and a histologically documented corneal irregularity has been established. The sensitivity and value of these signals in elucidating cellular/extracellular matrix changes in cornea and other thick tissues resulting from aberrant gene expression are also largely unknown.

We explored the potential of NLOM to detect genetically induced phenotypic alterations in the transgenic mouse model of corneal epithelial dysfunction. The modulation of Clim [co-factor of LIM (a combination of first letters of Lin-11 (*C. elegans*), ISL1 (rat), and Mec-3 (*C. elegans*) gene names) domain proteins, a diverse group of transcription factors] activity in epithelial tissues of mice using a keratin 14 (K14) promoter resulted in widespread epithelial abnormalities throughout the animal. The generation and characterization of these mice is discussed in a separate paper.¹⁵ The K14 domi-

Address all correspondence to Julia Lyubovitsky and Bruce J. Tromberg, Beckman Laser Institute, University of California, Irvine, 1002 Health Sciences Road, Irvine, CA 92612. Tel: (949) 824-4104; Fax: (949) 824-6969; E-mail: jlyubovi@uci.edu, bjtrombe@uci.edu

nant negative (DN)-Clim mice develop corneal abnormalities such that the corneas undergo an ultimate transformation into epidermis-like structures. These corneas become highly neovascularized, inflamed, and exhibit down-regulation of the corneal-specific protein keratin 12, concomitant with up-regulation of epidermal markers keratin 10, filaggrin, and loricrin in the epithelium.¹⁵ Eighty percent of mice are blind due to corneal opacities. In severe cases, the affected mice exhibit abnormal overgrowths of the stratified squamous epithelium, which are visually detectable and confirmed by histology.

In this work, endogenous cellular fluorescence and second harmonic signals from collagen showed dysplasia in the squamous epithelium, irregular collagen arrays in the stroma, and a compromised posterior endothelium in K14-DN-Clim mice corneas. A two-photon ratiometric redox fluorometry method based on cellular fluorescence from reduced nicotinamide adenine dinucleotide (NADH) and oxidized flavin adenine dinucleotide (FAD) indicated about 30% higher metabolic activity in the endothelial layer compared to an epithelial layer in both normal and aberrant corneas. Overall, the K14-DN-Clim mouse is an excellent model for NLOM to explore genetically induced corneal abnormalities ranging from cellular dysplasia to stromal matrix structural irregularities and neovascularization—processes commonly observed in cancer and fibrosis.

2 Materials and Methods

All animal procedures were performed in accordance with an animal protocol approved by the University of California at Irvine. Mice strain CB6F1 was used in all experiments. Transgenic mice were generated by microinjection of the suitable plasmid into fertilized eggs implanted into healthy CB6F1 animals. These mice expressed the transgene in the basal cell layer of the epidermis, the outer root sheath of hair follicles, the basal cell layer of neonatal corneal epithelium, and limbal cells of adult corneal epithelium.¹⁶ RNA isolation for microarray experiments were performed as described in Ref. 17. The microarrays data were analyzed using the software Cyber-T accessible through a Web interface¹⁸ (<http://www.genomics.uci.edu/software.html>) using a stringent statistical cut off value of 0.01.

2.1 Sample Preparation

All animals studied were euthanized by asphyxiation with CO₂. The ages of the mice were from two months up to one year. Mice eyes were removed, placed into 0.9% saline solution, and imaged immediately following euthanasia. The corneas were not dissected out of the eyes and were amenable to imaging for one or two hours. About 20 normal and 15 K14-DN-Clim mice eyes of matching ages were imaged.

2.2 Second Harmonic Generation/Two-Photon Fluorescence Imaging and Spectra

The images and spectra were obtained using a combined two-photon fluorescence (TPF)/second harmonic(SHG) setup previously described.^{9,12,19–27} The excitation was linearly polarized at 766 nm. Focusing objective (Zeiss, 63× water immersion, NA 1.2) was used to collect spectra and images. For photomultiplier tube (PMT) ratio imaging, a dichroic filter (500 nm) and bandpass filters [450±25 nm; NAD(P)H

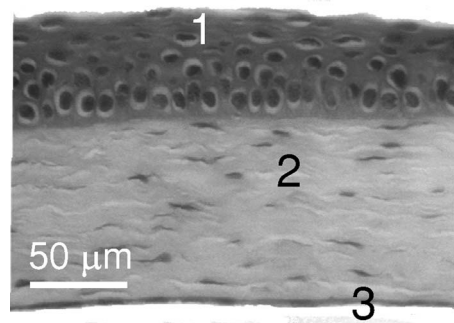


Fig. 1 H and E stained section of the normal mouse cornea. 1. Stratified squamous epithelium. 2. Stroma. 3. Posterior endothelium.

and 580±30 nm; flavoprotein] were used in front of corresponding PMTs. To minimize background signal from the laser, a broadband filter (320 to 660 nm) was placed in front of the spectrograph. The time for a typical *x-y* scan was one to three seconds. The spectra were collected from the single optical sections with the typical integration time of 15 sec; monochromator slit was 500 μm, and the laser beam was scanned continuously during spectral acquisition. The spectra were not corrected for the instrument response. The thickness of the corneas was measured with a long working distance focusing objective (Zeiss, 40× water immersion, NA 0.8).

2.3 Histological Evaluations

After remaining in saline for approximately 3 to 5 h during the NLOM imaging, specimens were fixed in 10% buffered formalin (Sigma-Aldrich, St. Louis, MO) overnight, dehydrated by an ethanol gradient, and embedded in paraffin wax (Fisher Scientific, Hampton, NH). The six micron sections closest to the center of the eye were stained with hematoxylin and eosin.

3 Results

3.1 Second Harmonic Generation/Two-Photon Fluorescence Signals and Spectra

Figure 1 shows a hematoxylin and eosin (H and E) stained, *en face* histology. Epithelium (the outer region of corneal tissue, top) is a layer about five cellular layers deep and contains 98% of nerve endings, making cornea very sensitive to pain.²⁸ Stroma (a layer behind epithelium) is the main component of cornea. Its composition is water, collagen fibers, and proteoglycans. The arrangement, spacing, and sizes of collagen fibers are critical in maintaining corneal transparency.²⁹ Endothelium (a single layer of cells located between the stroma and the aqueous humor) mainly functions to regulate water balance. All the topographic features seen in NLOM *x-y* scans (Fig. 2) have excellent coregistration with (H and E) stained sections; however, structural organization of collagen stroma evident in SHG/TPF images is not apparent in H and E processed tissues. Regardless of animal age, the corneal size was estimated to be around 150±10 μm from NLOM data, with the epithelial layer making up the first 50 μm, stroma with parallel arrangement of collagen layers comprising the next ~100 μm (Fig. 2), and endothelial layer at

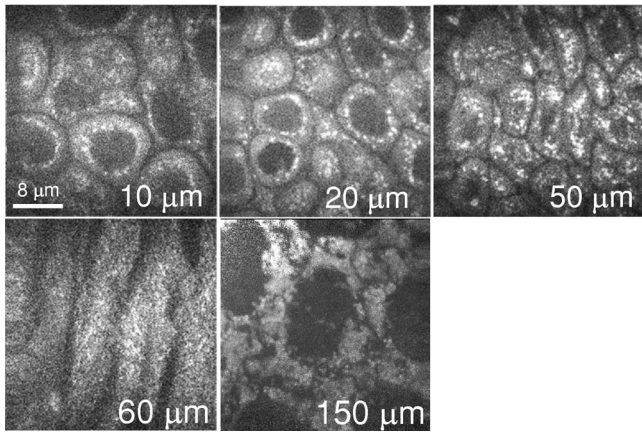


Fig. 2 Nonlinear optical signals (two-photon fluorescence and second harmonic generation) from a normal mouse cornea, *x-y* scans. The first 50 μm show the spatial organization of cells within the epithelial layer. At 60 μm , the parallel organization of collagen within stroma is observed. At 150 μm , the endothelial layer is present.

150 \pm 10 μm . The endothelial layer was the last layer amenable to imaging in reflectance, and no further SHG or TPF signals were detected with a physiology long-working-distance objective (Neofluar, model 440090, Zeiss, 40 \times water immersion, NA 0.8). The spectrum obtained for the normal mice eyes is a broad fluorescence band (Fig. 3). The two

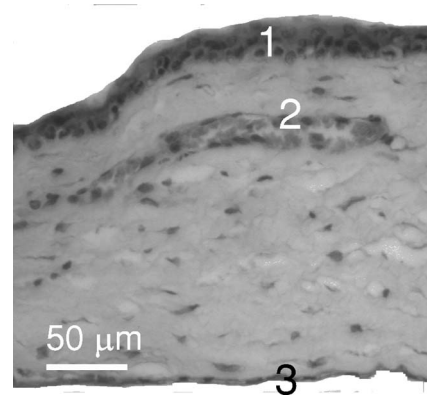


Fig. 4 H and E stained section of the K14-DN-Clim mouse cornea. 1. Epithelial cell dysplasia in the stratified squamous epithelium. 2. Cell invasion and neovascularization in stroma. 3. Posterior endothelium.

peaks at around 450 and 540 nm possibly result from NADH and FAD⁺ fluorescence, respectively (spectra not shown). The PMT ratio of the 450/540-nm peaks is 30% higher for the epithelial versus endothelial layer, which we believe is due to differences in metabolic activity between the two cellular layers. The spectrum of stroma is dominated by a second harmonic signal from collagen and was described earlier.¹²

Figure 4 shows a hematoxylin and eosin (H and E) stained, *en face* histology section for the moderately affected K14-

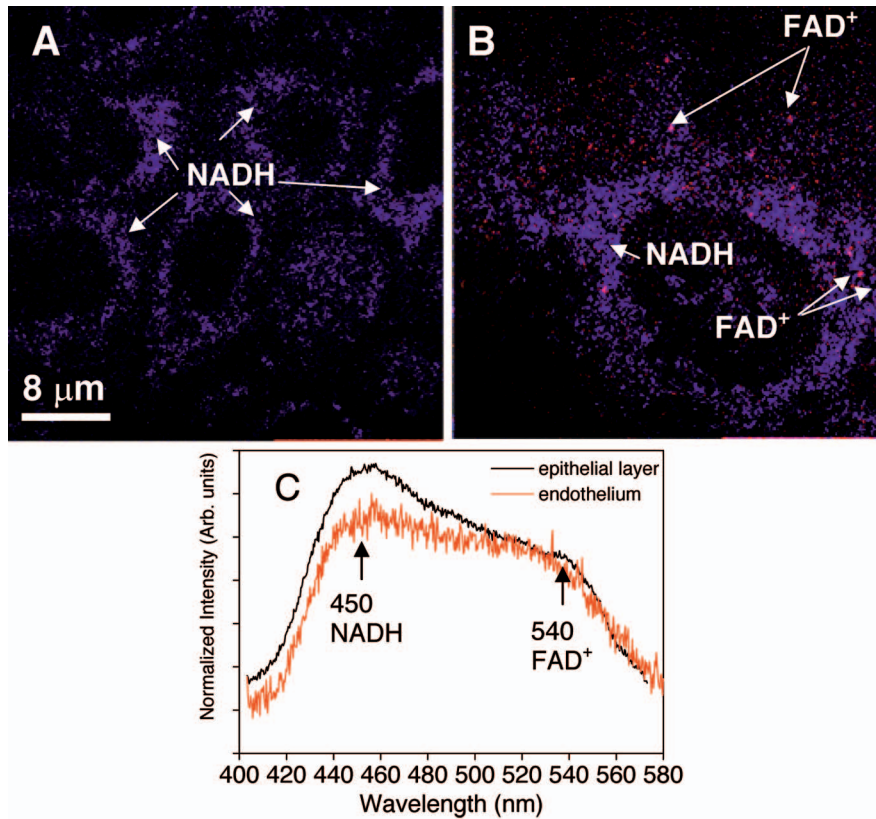


Fig. 3 Metabolic activity in the epithelial and endothelial layers of the normal mice corneas. (a) and (b) Color images consisting of two species: NADH (blue); FAD⁺ (pink). (a) Epithelial layer. (b) Endothelial layer. (c) Multiphoton excited fluorescence emission spectra from epithelial and endothelial layers. The spectra are not corrected for the instrument response.

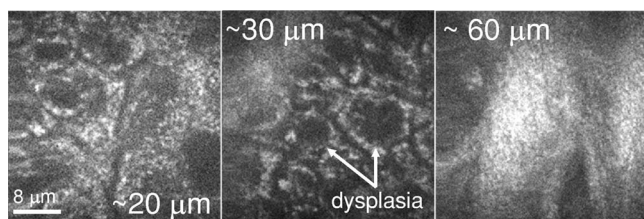


Fig. 5 Nonlinear optical signals (two-photon fluorescence and second harmonic generation) from a K14-DN-Clim mouse cornea, x - y scans. Dysplastic epithelium (center) and irregular collagen organization in the stroma (right) are clearly observed.

DN-Clim mice cornea. The high resolution NLOM images (Fig. 5) are highly effective in highlighting the dysplastic areas within the epithelial layer and irregular organization of collagen arrays within the stroma. In several severe cases, partial absence of the endothelial layer (differently sized cells show up in the same optical section) was also noted and confirmed by histology. When present, the endothelial cells were irregularly shaped. The spectrum for the K14-DN-Clim mice cornea is broad, with the PMT ratio of 450/540-nm peaks being 30% higher for the epithelial versus endothelial layer, similar to normal corneas.

4 Discussion

This work describes normal and pathological corneas in mice using reflectance NLOM (TPF and SHG combined). The epithelial layer dysplasia, irregularities in a collagen structure within stroma not apparent in H and E processed tissues, and compromised endothelial layer are reproducibly detected at high magnification in K14-DN-Clim mice corneas and validated with a conventional histology.

In many tumors, transformed epithelial cells are found to “prime” or provoke the microenvironment of extracellular matrix, which in turn undergoes dynamic alterations leading to structural changes, severe immune responses, and the formation of new blood vessels.³⁰ During this process, the fibrillar organization of extracellular matrix proteins such as fibronectin, collagen I, III, and V, elastin, and proteoglycans is modified,³¹ and their overall production is increased.³² In breast, the oncofetal extracellular matrix is usually thick, flaky, and largely disorganized.^{33,34} Altering the expression of the Clim gene in the epithelial tissues of mice resulted in corneas undergoing a continuous inflammatory/stromagenic/wound healing process concomitant with changes in the epithelial and endothelial cell layers. In line with up-regulation of many inflammatory markers¹⁵ and neovascularization in K14-DN-Clim mice corneas, based on mRNA microarray data (Fig. 6), procollagen III production is increased at least 2.5 fold compared to a healthy mouse. We therefore propose that the irregular appearance of the stromal collagen in the NLOM images of K14-DN-Clim mice corneas is due to reorganization of extracellular matrix and deposition of smaller, disorganized fibrils perhaps associated with collagen III. While collagen I is the major fibrillar component of the cornea, it is not actively synthesized in healthy adult corneas. Collagen III is commonly overproduced in response to inflammation/wound healing in skin³⁵ and in cornea^{36–39} by the stromal keratocytes that transdifferentiate into fibroblasts and

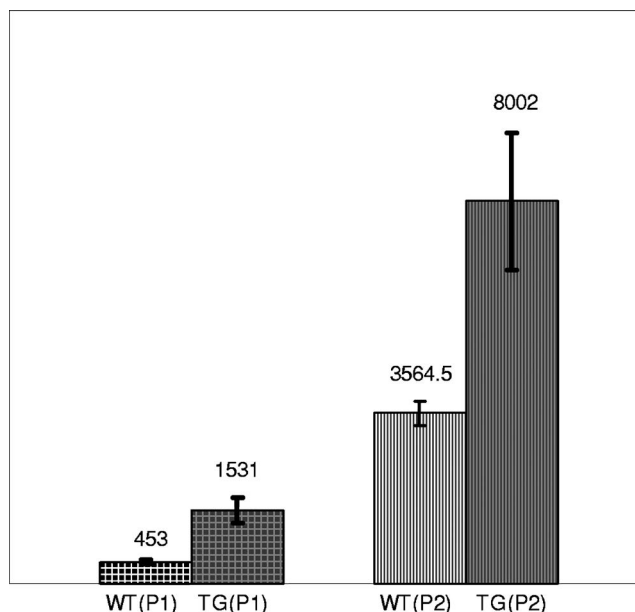


Fig. 6 Procollagen, type III, alpha 1 mRNA expression is up-regulated in K14-DN-Clim mice. Data from Affymetrix microarrays for normal (WT) and transgenic (TG) mice corneas using two probe sets (P1, P2). The bars and numbers are the means; the error bars are the standard errors of the mean based on sample standard deviations.

myofibroblasts.⁴⁰ It is deposited with disorganized architecture, providing a framework for collagen I fibers⁴¹ observed in the later stages of wound repair.

Most K14-DN-Clim mice develop obvious macroscopic evidence of corneal abnormalities around six weeks of age. However, partial loss of Clim function leads to a complex phenotype with a severity of the condition varying greatly among individuals of the same age. To overcome the challenge of detecting early stages in K14-DN-Clim mice corneal pathology, we are currently implementing live animal imaging.

Two-photon ratiometric redox fluorometry based on cellular fluorescence from reduced nicotinamide adenine dinucleotide (NADH) and oxidized flavin adenine dinucleotide (FAD) has been proposed as a tool to study mitochondrial energy metabolism.⁴² Only reduced NADH and oxidized FAD states of these cofactors are significantly fluorescent and linked through the NADH-Q-reductase and various dehydrogenases⁴³ in a process known as oxidative phosphorylation (OXPHOS). They will respond differently to changes in mitochondrial metabolic states, and a ratio NADH/FAD⁺ will be a measure of mitochondrial energetics. Several earlier studies used fluorescence of NAD(P)H^{11,44} and flavoprotein to address the mitochondrial energy metabolism in the biological systems.^{45–53} Our two-photon ratiometric imaging results indicate a higher metabolic activity in the endothelial layer of cornea compared to an epithelial layer located further away from metabolites. An observed difference of 30% might be even greater *in vivo*, where the endothelial layer conducts metabolite exchange and actively regulates water balance at physiological temperatures. Earlier observations of flavoprotein/NADH and NAD(P)H signals obtained from single photon excitation of perfused corneas detected ~50%

higher metabolic rate for endothelium relative to that of epithelium.^{11,44,47} Tissue handling associated with *ex-vivo* measurements is likely to influence our two-photon ratiometric redox fluorometry measurements by inducing a shut down of endothelial layer function in about an hour at room temperature. Therefore, we are currently investigating the utility of functional corneal imaging on live animals.

5 Conclusions

High-resolution reflectance-based NLOM methods offer novel approaches to probe the downstream effects of gene expression and their influence on phenotypes *in vivo* without use of exogenous dyes. In this study, the *Clim* gene is partially blocked in the epithelial compartment of mice tissues: however, it causes significant structural changes in corneal stroma, indicating that *Clims* may be involved in epithelial-mesenchymal interactions. We detect these changes at high magnification using nondestructive NLOM imaging, and on comparison to normal stromas shows that the method is effective in detailing structural pathologies in reorganized extracellular matrix. These extracellular matrix structural alterations are likely due to collagen III synthesis and deposition during healing and remodeling of corneal stroma. Because no exogenous dyes are employed, NLOM visualization can be used in selecting tissues for gene expression profiling. In addition, NLOM ratiometric redox fluorometry results provide preliminary confirmation that cellular metabolic function can be characterized and imaged in thick tissues.

Acknowledgments

Julia G. Lyubovitsky thanks George E. Hewitt and the George E. Hewitt Foundation for Medical Research for the fellowship. This work was made possible, in part, through the NIH Laser Microbeam and Medical Program (LAMMP) at the University of California, Irvine (P41-RR01192) and by the Air Force Office of Scientific Research (AFOSR), under agreement number FA9550-04-1-0101. Bogi Andersen is supported by NIH grant AR44882.

References

1. D. M. Maurice, "The structure and transparency of the cornea," *J. Physiol. (London)* **136**, 268–286 (1957).
2. P. J. Campagnola, M. D. Wei, A. Lewis, and L. M. Loew, "High-resolution nonlinear optical imaging of live cells by second harmonic generation," *Biophys. J.* **77**, 3341–3349 (1999).
3. P. J. Campagnola, H. A. Clark, W. A. Mohler, A. Lewis, and L. M. Loew, "Second-harmonic imaging microscopy of living cells," *J. Biomed. Opt.* **6**(3), 277–286 (2001).
4. L. Moreaux, O. Sandre, M. Blanchard-Desce, and J. Mertz, "Membrane imaging by simultaneous second-harmonic generation and two-photon microscopy," *Opt. Lett.* **25**, 320–322 (2000).
5. L. Moreaux, O. Sandre, S. Charpack, M. Blanchard-Desce, and J. Mertz, "Coherent scattering in multi-harmonic light microscopy," *Biophys. J.* **80**, 1568–1574 (2001).
6. R. Gauderon, P. B. Lukins, and S. J. Sheppard, "Optimization of second-harmonic generation microscopy," *Micron* **32**, 691–700 (2001).
7. P. J. Campagnola, A. C. Millard, M. Terasaki, P. E. Hoppe, C. J. Malone, and W. A. Mohler, "Three-dimensional high resolution second-harmonic generation imaging of endogenous structural proteins in biological tissues," *Biophys. J.* **82**, 493–508 (2002).
8. Y. Guo, H. E. Savage, F. Liu, S. P. Schantz, P. P. Ho, and R. R. Alfano, "Subsurface tumor progression investigated by noninvasive optical second harmonic tomography," *Proc. Natl. Acad. Sci. U.S.A.* **96**, 10854–10856 (1999).
9. A. Zoumi, A. Yeh, and B. J. Tromberg, "Imaging cells and extracellular matrix *in vivo* by using second-harmonic generation and two-photon excited fluorescence," *Proc. Natl. Acad. Sci. U.S.A.* **99**, 11014–11019 (2002).
10. E. Brown, T. McKee, E. DiTomaso, A. Pluen, B. Seed, and Y. Boucher, "Dynamic imaging of collagen and its modulation in tumors *in vivo* using second-harmonic generation," *Nat. Med.* **9**, 796–801 (2003).
11. D. W. Piston, B. Masters, and W. W. Webb, "Three-dimensionally resolved NAD(P)H cellular metabolic redox imaging of the *in situ* cornea with two-photon excitation laser scanning microscopy," *J. Microsc.* **178**, 20–27 (1995).
12. A. T. Yeh, N. Nassif, A. Zoumi, and B. J. Tromberg, "Selective corneal imaging using combined second-harmonic generation and two-photon excited fluorescence," *Opt. Lett.* **27**, 2082–2084 (2002).
13. M. Han, L. Zickler, G. Giese, M. Walter, F. H. Loesel, and J. F. Bille, "Second-harmonic imaging of cornea after intrastromal femtosecond laser ablation," *J. Biomed. Opt.* **9**(4), 760–766 (2004).
14. M. Han, G. Giese, L. Zickler, H. Sun, and J. F. Bille, "Mini-invasive corneal surgery and imaging with femtosecond lasers," *Opt. Express* **12**, 4275–4281 (2004).
15. X. Xu, J. A. Spencer, K. K. Lin, E. I. Kudryavtseva, and B. Andersen, "Characterization of mice expressing a dominant negative *Clim* in epithelial tissues," (to be published).
16. Limbal epithelium is where the corneal epithelium stem cells are believed to be located.
17. K. K. Lin, D. Chudova, G. W. Hatfield, P. Smyth, and B. Andersen, "Identification of hair cycle-associated genes from time-course gene expression profile data by using replicate variance," *Proc. Natl. Acad. Sci. U.S.A.* **101**, 15955–15960 (2004).
18. P. Baldi and A. D. Long, "A Bayesian framework for the analysis of microarray expression data: regularized t-test and statistical inferences of gene changes," *Bioinformatics* **17**, 509–519 (2001).
19. A. Agarwal, M. L. Coleno, V. P. Wallace, W. Y. Wu, C. H. Sun, B. J. Tromberg, and S. C. George, "Two-photon laser scanning microscopy of epithelial cell-modulated collagen density in engineered human lung tissue," *Tissue Eng.* **7**, 191–202 (2001).
20. A. K. Dunn, V. P. Wallace, M. Coleno, M. W. Berns, and B. J. Tromberg, "Influence of optical properties on two photon fluorescence imaging in turbid samples," *Appl. Opt.* **39**, 1194–1201 (2000).
21. T. F. Kelly, F. M. Sutton, V. P. Wallace, and B. J. F. Wong, "Chondrocyte repopulation of allograft cartilage: A preliminary investigation and strategy for developing cartilage matrices for reconstruction," *Otolaryngol.-Head Neck Surg.* **127**, 256–270 (2002).
22. V. J. LaMorte, A. Zoumi, and B. J. Tromberg, "Spectroscopic approach for monitoring two-photon excited FRET from homodimers at the subcellular level," *J. Biomed. Opt.* **8**(3), 357–361 (2003).
23. B. J. F. Wong, V. Wallace, M. Coleno, H. P. Benton, and B. J. Tromberg, "Two-photon excitation laser scanning microscopy of human, porcine, and rabbit nasal septal cartilage," *Tissue Eng.* **7**, 599–606 (2002).
24. A. T. Yeh, B. Choi, J. S. Nelson, and B. J. Tromberg, "Reversible dissociation of collagen in tissues," *J. Invest. Dermatol.* **121**, 1332–1335 (2003).
25. A. T. Yeh, B. S. Kao, W. G. Jung, Z. P. Chen, J. S. Nelson, and B. J. Tromberg, "Imaging wound healing using optical coherence tomography and multiphoton microscopy in an *in vitro* skin-equivalent tissue model," *J. Biomed. Opt.* **9**(2), 248–253 (2004).
26. A. Zoumi, "Optimization of imaging depth and spectral content in multiphoton microscopy," PhD Thesis, Biomedical Engineering, Univ. California, Irvine, p. 202 (2003).
27. A. Zoumi, X. Lu, G. S. Kassab, and B. J. Tromberg, "Imaging coronary artery microstructure using second-harmonic and two-photon fluorescence microscopy," *Biophys. J.* **87**, 2778–2786 (2003).
28. D. M. Maurice, "Clinical physiology of the cornea," *Int. Ophthalmol. Clin.* **2**, 561–572 (1962).
29. Collagen fibrils in the corneal stroma of mice are uniformly thin at about 32 nm in diameter and arranged in lamellae; K. M. Meek, A. J. Quantock, C. Boote, C.-Y. Liu, and W. W.-Y. Kao, "An x-ray scattering investigation of corneal structure in keratan-deficient mice," *Matrix Biol.* **22**, 467–475 (2003).
30. E. Cukierman, "A visual-quantitative analysis of fibroblastic stromagenesis in breast cancer progression," *J. Mammary Gland Biol. Neoplasia* **9**, 311–324 (2004).
31. T. Silzle, G. J. Randolph, M. Kreutz, and L. A. Kunz-Schughart,

- "The fibroblast: Sentinell cell and local immune modulator in tumor tissue," *Int. J. Cancer* **108**, 173–180 (2004).
32. A. Noel, F. Kebers, E. Maquoi, and J. M. Foidart, "Cell-cell and cell-matrix interactions during breast cancer progression," *Curr. Top Pathol.* **93**, 183–193 (1999).
 33. Y. C. Wong, and N. N. Tam, "Dedifferentiation of stromal smooth muscle as a factor in prostate carcinogenesis," *Dedifferentiation* **70**, 633–645 (2002).
 34. L. A. Kunz-Schughart and R. Knuechel, "Tumor-associated fibroblasts (Part I): Active stromal participants in tumor development and progression?" *Histol. Histopathol* **17**, 599–621 (2002).
 35. J. N. Clore, I. K. Cohen, and R. F. Diegelmann, "Quantitation of collagen types I and III during wound healing in rat skin," *Proc. Soc. Exp. Biol. Med.* **161**, 337–340 (1979).
 36. C. Cintron, B. S. Hong, H. I. Covington, and E. J. Macarak, "Heterogeneity of collagens in rabbit cornea: type III collagen," *Invest. Ophthalmol. Visual Sci.* **29**, 767–775 (1988).
 37. J. A. Anderson, P. S. Binder, M. E. Rock, and M. P. Vrabc, "Human excimer laser keratectomy. Immunohistochemical analysis of healing," *Arch. Ophthalmol. (Chicago)* **114**, 54–60 (1996).
 38. D. S. Malley, R. F. Steinert, C. A. Puliafito, and E. T. Dobi, "Immunofluorescence study of corneal wound healing after excimer laser anterior keratectomy in the monkey eye," *Arch. Ophthalmol. (Chicago)* **108**, 1316–1322 (1990).
 39. C. Chen, B. Michelini-Norris, S. Stevens, J. Rowsey, X. Ren, M. Goldstein, and G. Schultz, "Measurement of mRNAs for TGF β and extracellular matrix proteins in corneas of rats after PRK," *Invest. Ophthalmol. Visual Sci.* **41**, 4108–4116 (2000).
 40. J. L. Funderburgh, M. M. Mann, and M. L. Funderburgh, "Keratocyte phenotype mediates proteoglycan structure (A role for fibroblasts in corneal fibrosis)," *J. Biol. Chem.* **278**, 45629–45637 (2003).
 41. Collagen fibrils in the corneal stroma are type I/type V hybrids; D. E. Birk, J. M. Fitch, J. P. Babiartz, and T. F. Linsenmayer, "Collagen type I and type V are present in the same fibril in the avian corneal stroma," *J. Cell Biol.* **106**, 999–1008 (1998).
 42. S. Huang, A. A. Heikal, and W. W. Webb, "Two-photon fluorescence spectroscopy and microscopy of NAD(P)H and Flavoprotein," *Biophys. J.* **82**, 2811–2825 (2002).
 43. C. A. Combs and R. S. Balaban, "Direct imaging of dehydrogenase activity within living cells using enzyme-dependent fluorescence recovery after photobleaching (ED-FRAP)," *Biophys. J.* **80**, 2018–2028 (2001).
 44. B. Masters, M. V. Riley, J. Fischbarg, and B. Chance, "Pyridine nucleotides of rabbit cornea with histotoxic anoxia: Chemical analysis, non-invasive fluorometry and physiological correlates," *Exp. Eye Res.* **37**, 1–9 (1983).
 45. B. Chance, P. Cohen, F. Jobsis, and B. Schoener, "Intracellular oxydation-reduction states *in vivo*," *Science* **137**, 499–508 (1962).
 46. B. Chance, I. A. Salkovitz, and A. G. B. Kovach, "Kinetics of mitochondrial flavoprotein and pyridine nucleotide in perfused heart," *Am. J. Phys.* **223**, 207–218 (1972).
 47. B. Chance and M. Lieberman, "Intrinsic fluorescence emission from the cornea at low temperatures: Evidence of mitochondrial signals and their differing redox states in epithelial and endothelial sides," *Exp. Eye Res.* **26**, 111–117 (1978).
 48. W. Kunz and W. Kunz, "Contribution of different enzymes to flavoprotein fluorescence in isolated rat liver mitochondria," *Biochim. Biophys. Acta* **841**, 237–246 (1985).
 49. B. R. Masters, P. T. C. So, and E. Gratton, "Optical biopsy of *in vivo* human skin: Multiphoton excitation microscopy," *Lasers Med. Sci.* **13**, 196–203 (1998).
 50. D. N. Romashko, E. Marban, and B. O'Rourke, "Subcellular metabolic transients and mitochondrial redox waves in heart cells," *Proc. Natl. Acad. Sci. U.S.A.* **95**, 1618–1623 (1998).
 51. A. V. Kuznetsov, O. Mayboroda, D. Kunz, K. Winkler, W. Schubert, and W. S. Kunz, "Functional imaging of mitochondria in saponin-permeabilized mice muscle fibers," *J. Cell Biol.* **140**, 1091–1099 (1998).
 52. A. V. Kuznetsov, Y. Ussov, X. Leverage, and R. Margreiter, "Subcellular heterogeneity of mitochondrial function and dysfunction: Evidence obtained by confocal imaging," *Mol. Cell. Biochem.* **256**, 359–365 (2004).
 53. A. C. Croce, A. Ferrigno, M. Vairetti, R. Bertone, I. Freitas, and G. Bottiroli, "Autofluorescence properties of isolated rat hepatocytes under different metabolic conditions," *Photochem. Photobiol. Sci.* **3**, 920–926 (2004).